PAPER

Check for updates

Pyridoxal-based low molecular weight progelator as a new chemosensor for the recognition of Ag+ and Hg2+ under different conditions†

Saswati Ghosh Roy,[a] Abhishek Kumar, [iD][b] Neeraj Misra [iD][b] and
Kumaresh Ghosh [iD] *[a]

Pyridoxal-based low molecular weight progelator **1** has been designed and synthesized for the selective visual detection of Ag+ ions through sol-to-gel conversion. Compound **1** shows excellent gelation property with desired gel stiffness only in the presence of Ag+ ions over a series of other metal ions in 1:1 (v/v) aqueous solvent system miscible with organic solvents such as DMSO, DMF, and dioxane, and validates the visual detection of Ag+ ions. The gel properties were studied by FTIR, UV-Vis, scanning electron microscopy (SEM), and rheology measurements. Minimum gelation concentration was found to be 3 mg mL^{-1}. While Ag+-induced metallogel in DMSO/H$_2$O is thermally reversible, it is irreversible in the DMF/H$_2$O system. The model compound **2**, devoid of hydroxyl groups, did not show gelation under identical conditions and established the role of pyridoxal moiety in **1**. In addition, compound **1** exhibits the selective sensing of Hg^{2+} ions over a series of metal ions in the solution phase, as established by UV-Vis, fluorescence, and ^{1}H NMR studies.

Introduction

Low molecular weight gelators (LMWGs) or supramolecular gelators are an interesting and useful class of materials. The development of LMWGs for the construction of supramolecular gels and their subset, metallogels, have received immense interest in recent years due to their potential applications in a wide range of fields, including cell culture,[1,2] tissue engineering,[3,4] wound healing,[5] water purification,[6,7] drug delivery,[8,9] sensing and catalysis,[10,11] and optoelectronics.[12,13] These gels are viscoelastic semisolid materials that are formed owing to the self-assembly of small molecules into a large anisotropic three-dimensional (3D) network that entraps a large volume of solvent molecules. The driving forces for the formation of such a stable 3D network are π–π stacking, H-bonding, van der Waals force, dipole–dipole interaction, presence of coordinating analytes, *etc.*[14,15] The development of LMWGs-containing metal ion binding groups may provide

the additional advantage of being stimuli responsive in nature.[16]

It is established that metal-assisted supramolecular assemblies are of great interest due to their applications in sensing,[17] catalysis,[18] magnetic fields,[19] optics,[20] *etc.* Furthermore, metal ion inclusion into LMWGs, leading to the formation of a new hybrid material with ion conducting properties, can be useful in supercapacitors,[21,22] solar cells,[23] rechargeable batteries,[24] fuel cells,[25] *etc.* Importantly, among the various uses, the sensing of metal ions by LMWGs in aqueous and semi-aqueous media is an important area of research in environmental and supramolecular chemistry.
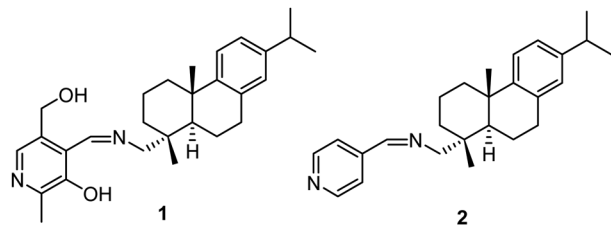
Herein, we report the design, synthesis, and characterization of low molecular weight Schiff bases **1** and **2** derived from the condensation of dehydroabietylamine with pyridoxal and pyridine-4-carboxaldehyde, respectively (Fig. 1). Compound **1** acted as a progelator and showed excellent gelation only in the presence of Ag+ ions over a series of other metal ions in 1:1 (v/v) aqueous solvent miscible with organic solvents such as DMSO, DMF, and dioxane. Besides, in solution phase (DMSO/H$_2$O, 1/1, v/v), compound **1** showed the selective detection of Hg^{2+} ion over a series of other metal ions. Schiff base **2** as a model compound was employed in a similar study and did not produce the gel either alone or in the presence of metal ions. This demonstrated the role of pyridoxal in gel formation in **1**.

Among various toxic metal ions, Hg^{2+} is a soft and toxic metal ion, which has adverse effect on human health as well as

[a] *Department of Chemistry, University of Kalyani, Kalyani 741235, India.*
 E-mail: ghosh_k2003@yahoo.co.in, kumareshchem18@klyuniv.ac.in;
 Fax: +913325828282; Tel: +913325828750; Extn. 305
[b] *Department of Physics, University of Lucknow, Lucknow 226007, India*
† Electronic supplementary information (ESI) available: Gelation study, Fig. showing change in fluorescence and UV-vis, theoretical UV-vis plots, binding curve and detection limit, spectral data, TEM, CD spectra, rheology, comparison table. See DOI: https://doi.org/10.1039/d2ma00358a
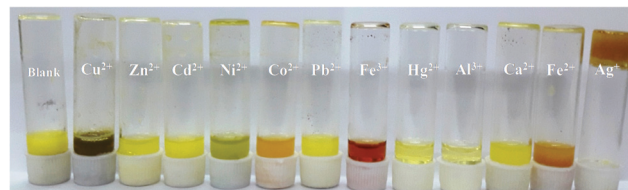
Fig. 1 Structures of **1** and **2**.

Fig. 2 Photograph showing the sol–gel transition of **1** (c = 0.023 mol) upon the addition of 1 equiv. amount of various metal salts (c = 0.046 mol) in DMSO/H$_2$O (1:1, v/v). All metal salts were taken as their nitrate salts (NO$_3^-$) except Hg^{2+}, Fe^{2+}, and Al^{3+}, which were taken as their perchlorate salts (ClO$_4^-$).

environment.[26] It causes serious damage to lung, heart, kidney, brain, and human immune system. Organic mercury causes Minamata and coronary heart diseases.[27] On the other hand, Ag$^+$ is a biologically important ion due to its antimicrobial activity.[28] It finds great application in organic synthesis,[29] catalysis,[30] electronic,[31] photography,[32] imaging industry,[33] *etc.* Recently, the application of LMWGs for the recognition of such toxic/heavy metal ions has attracted much interest owing to the simple naked eye detection involving sol-to-gel conversion or *vice versa*.[34] To date, reports on LMWGs-based recognition of toxic/heavy metal ions are limited[35] due to the lack of desired sufficient stiffness of gels and also the lack of sensitivity and selectivity. In this context, the present report is concerned with the development of a simple LMWG for the naked eye recognition of toxic and/or heavy metal ions through the formation of a stable gel.

Results and discussion

Synthesis

Compound **1** was obtained as a yellow solid in an appreciable yield from the condensation of dehydroabietylamine with pyridoxal (obtained from pyridoxal hydrochloride) (Scheme 1). Model compound **2** was obtained as a colorless gummy material in 70% yield from the condensation of dehydroabietylamine with pyridine-4-carboxaldehyde (Scheme 1). Both compounds **1** and **2** were characterized by ^{1}H NMR, ^{13}C NMR, FT IR, and mass analysis (Fig. S1–S5, ESI†).

Gelation study

The gelation property of compound **1** was tested in a wide range of organic solvents (Table S1, ESI†) by the typical inversion of the vial method. Compound **1** did not form a gel in any of the tested solvents and remained soluble in all tested organic solvents (toluene, benzene, THF, DMSO, CH$_3$CN, CH$_3$OH, DCM, *etc.*). Compound **1** was insoluble in water due to the presence of a dehydroabeityl moiety that provides hydrophobic

surface. Therefore, it was anticipated that gelation might occur in organic solvent mixture using water as the co-solvent. However, precipitation was observed from mixed solvents instead of gel formation (Table S1, ESI†). As compound **1** contains a pyridine nucleus, it was further anticipated that it might form a gel in the presence of suitable metal ions. Thus, the gelation of **1** was tested in dioxane/H$_2$O (1:1, v/v), DMSO/H$_2$O (1:1, v/v), and DMF/H$_2$O (1:1, v/v) mixture solvents in the presence of different metal ions (Fig. 2). Importantly, only in the presence of Ag$^+$ ions, gelation occurred within a few seconds in all aqueous organic mixture solvents (Table S1, ESI†). Ag$^+$-induced gelation was also observed in CH$_3$CN/H$_2$O (1:1, v/v) after 10 min. Such a type of gelation of progelator **1** is a smart approach for developing molecular sensor for the naked-eye detection of chemical analytes.[36] To demonstrate this, we selected DMSO/H$_2$O (1:1, v/v) solvent system for further investigation.

The effect of different metal salts on the gelation of progelator **1** is shown in Fig. 2. In the study, aqueous solutions of different metal salts were added separately in 2 equiv. amounts to the solution of **1** in DMSO. It was only Ag$^+$ ion that induced the gelation of **1** immediately. Any sol–gel transition of **1** was not observed in the presence of other metal ions (Cu^{2+}, Zn^{2+}, Cd^{2+}, Ni^{2+}, Co^{2+}, Pb^{2+}, Fe^{3+}, Hg^{2+}, Al^{3+}, Ca^{2+}, and Fe^{2+}) even after 1 h. There were color changes of the solution in the presence of some metal ions. Fe^{3+}-induced red coloration of the solution was distinctive in this regard. However, gelation of **1** was also observed in the presence of 1 equiv. amount of Ag$^+$ ion, but it was delayed by 15 min. However, in the presence of 0.9 equiv. of Ag$^+$, a gel-like mass was observed in the vial although it was not stable. We further studied the gelation of **1** in the presence of 0.5 equivalent of Ag$^+$ ion. maintaining a 2:1 (ligand:metal ion) stoichiometry and in this case, no gel was formed after 1 h (Fig. S6, ESI†). These observations on gel formation established the sensitivity and high selectivity of compound **1** toward Ag$^+$ ion over the other metal ions studied.

To study the effect of the counter anion in Ag$^+$ salt on the phase transition of **1**, three different Ag$^+$ salts such as AgNO$_3$, AgOAc, and AgClO$_4$ were taken. Instant gelation was observed in the presence of both AgNO$_3$ and AgClO$_4$, whereas sol-to-gel transition of **1** was delayed by 30 min in the presence of AgOAc (Fig. 3). This reveals that AcO$^-$ has some kinetic effect on gelation. The acid-base interaction of AcO$^-$ ion with the
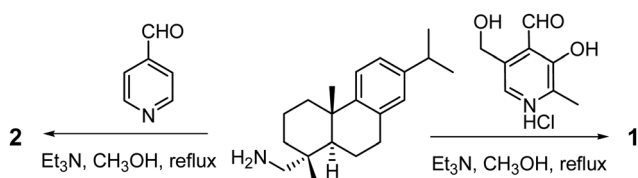
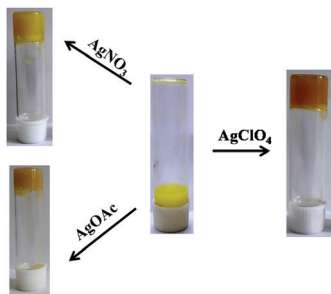Scheme 1 Syntheses of compounds **1** and **2**.

Fig. 3 Gelation study of compound **1** (5 mg mL^{-1}) in DMSO–H$_2$O (v/v, 1/1) in the presence of AgNO$_3$, AgOAc, and AgClO$_4$.

phenolic OH is considered to be the cause of such observation. The rheological property of this gel, which is described later in this section, is observed to be different from the gel derived from AgNO$_3$.

The minimum gelation concentration of **1** was found to be 3 mg mL^{-1} in the presence of 1 equiv. amount of Ag$^+$. Lowering this concentration did not show any sol-to-gel transition of **1** even after 1 h in the presence of 1 equiv. amount of Ag$^+$.

To understand the nature of aggregation of compound **1** in the presence of Ag$^+$, the comparison of the UV-vis spectra of **1** in solution and gel states was done (Fig. 4). The absorption peak of **1** at 336 nm in DMSO–H$_2$O (v/v, 1/1) was red-shifted to 346 nm and the intense absorption at 418 nm, possibly due to the partial deprotonation of the phenolic –OH in solution, was reduced significantly with broadening in the gel state. This occurred presumably due to H-bond-induced aggregation involving –OH groups of the pyridoxal moiety and also hydrophobic interaction exerted by the dehydroabietyl group. In fluorescence, the emissions at ~400 nm and ~540 nm in the sol state are reduced compared with the gel state. Such an observation in fluorescence may be due to the aggregation-induced quenching of emission.

The aggregation behavior of compound **1** in the presence of Ag$^+$ was further supported by FTIR analysis. The FTIR spectra of **1** both in amorphous and gel states were recorded and compared. The stretching signal at 3360 cm^{-1} due to the –OH groups of the pyridoxal in the amorphous state was considerably broadened in the gel state due to extensive hydrogen bonding also involving water. As a consequence, the stretching at 1623 cm^{-1} for the imine bond (C=N) in the amorphous state was shifted to 1662 cm^{-1} in the gel state seemingly due to its
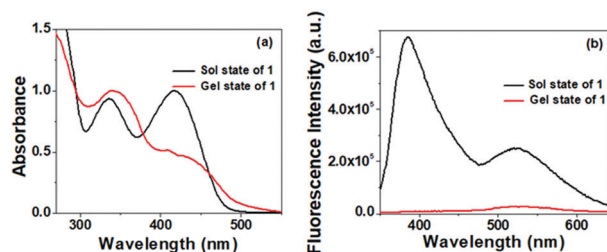

Fig. 4 Comparison of (a) normalized UV-vis and (b) fluorescence spectra of **1** in the solution [DMSO/H$_2$O (1:1, v/v)] and gel states.
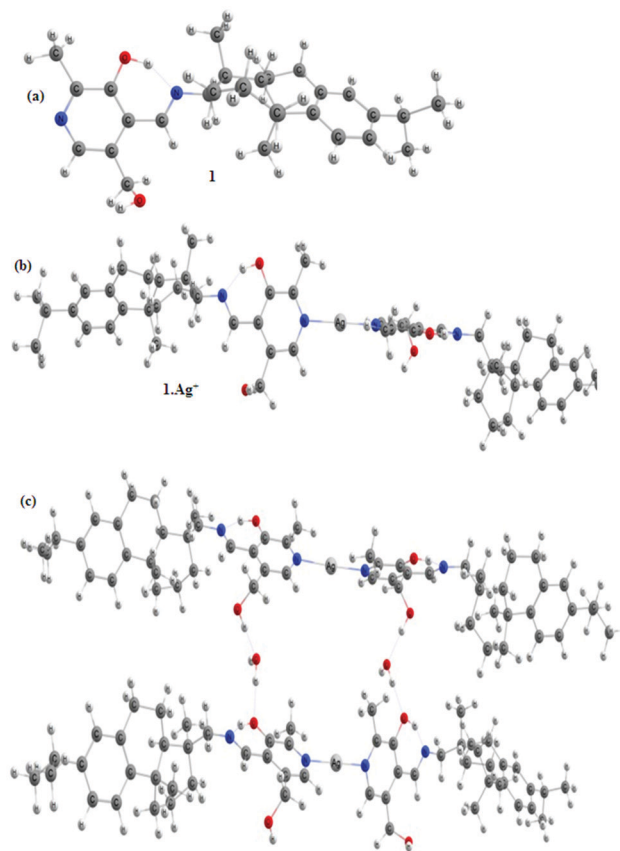

Fig. 5 Optimized geometries of (a) compound **1**, (b) compound **1** with Ag$^+$, and (c) tetramer of compound **1** with two Ag$^+$ ions in DMSO solvent calculated at the DFT/B3LYP 6-311++G(d,p) level.

restricted rotation in the gel state (Fig. S7, ESI†). In addition, a broad signal at ~2000 cm^{-1} in the gel state was a proof of involvement of the pyridine ring nitrogen in interaction.

To realize the role of the pyridoxal motif in the gel formation, model compound **2** was considered in the study. Compound **2** is almost similar to **1**, where the pyridoxal moiety is replaced by pyridine. Without –OH groups, compound **2** was unable to form a gel in the presence of any metal ion under similar conditions (Fig. S8, ESI†).

However, we were keen to investigate the aggregation mode of **1** during gelation; in this regard, we performed the DFT study.[37] Geometry optimization of **1** shows that while the imine part is engaged in intramolecular H-bonding with the phenolic–OH, the pyridine ring nitrogen is free for metal ion coordination (Fig. 5(a)). Fig. 5(b) depicts the Ag$^+$-coordinated complex in DMSO where there is a slight conformational change after binding with the silver ion. The presence of water involves hydrogen bonding with the alcoholic group and encourages the aggregation. In this regard, the tetrameric form of the complex considered to understand the possible mode of aggregation during gelation. To substantiate this, the absorption spectra were recorded. In this regard, the absorption peak at 311 nm for the tetrameric aggregated form in Fig. 5(c) was found to be nearer to the peak at 346 nm for the gel state in Fig. 4(a) and

(Fig. S9, ESI†). To explain the absorption peak at 418 nm for **1** in DMSO, the TDDFT calculation on the deprotonated form of **1** (deprotonation of the phenolic –OH) was done. Importantly, the peak at 412 nm for this closely matched with the experimental value (Fig. S10, ESI†) and confirmed the existence of the phenoxide form in solution.

The frontier molecular orbitals (FMO), highest occupied molecular orbital (HOMO), and lowest unoccupied molecular orbital (LUMO) of **1** and its complex structures are shown in Fig. S11–S13 (ESI†). FMOs determine the way the molecule interacts with other species and the gap between these also helps in characterizing the chemical reactivity and kinetic stability of the molecule. The calculated value of the HOMO–LUMO gap shows a decrease of 0.51 eV in complex formation in comparison to the free ligand (compound **1**), *i.e.*, the complex structure is more reactive than the free ligand.

The molecular electrostatic surface potential (MESP) was plotted to investigate the reactive sites in the studied compounds. The MESP plot simultaneously displays the molecular size, shape, as well as positive, negative, and neutral electrostatic potential regions in terms of the color grading. In the MESP plot of complex structures (Fig. 6(a) and (b)), the most electropositive region (blue region, electron poor) is located over the side where the N-atom is attached to the silver ion, while there is no electronegative region present in the structures. Thus, the complex system appears to be profoundly sensitive toward nucleophilic species, for which there will be gelation through a network formation.

Thermal behavior, surface morphology, and CD spectra of the metallogel

To study the thermal stability of the Ag⁺–gel, T_{gel} was measured for both the Ag⁺-induced gels of compound **1** in DMSO/H$_2$O (v/v, 1/1) and DMF/H$_2$O (v/v, 1/1). Importantly, the gel obtained in DMF/H$_2$O (5 mg mL^{-1}, T_{gel} = 82 °C) was much thermally
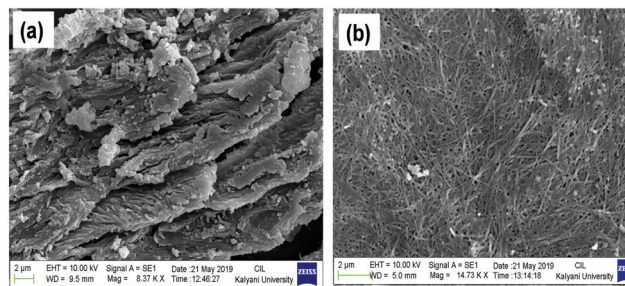
Fig. 7 The SEM image of xerogel of compound **1** prepared in DMSO/H$_2$O (1 : 1, v/v) in the presence of (a) 1 equiv. and (b) 2 equiv. of Ag⁺ ion.

stable than the gel in DMSO/H$_2$O (5 mg mL^{-1}, T_{gel} = 62 °C). However, the gel obtained in the DMF/H$_2$O solvent system was not thermally reversible (Fig. S14a, ESI†), whereas the gel in DMSO/H$_2$O showed reversible sol-to-gel phase transition (Fig. S14b, ESI†).

The surface morphology of the Ag⁺ gel was investigated by the SEM imaging technique. Xerogel of **1** obtained from 1 equiv. of Ag⁺ in DMSO/H$_2$O showed uneven cluster formation, whereas the xerogel obtained from 2 equiv. of Ag⁺ showed highly crosslinked fibrous network structure (Fig. 7). The TEM micrograph of xerogel of **1** prepared in DMSO/H$_2$O (1 : 1, v/v) in the presence of 2 equiv. of Ag⁺ ion showed a network structure formed with uneven void space due to the aggregation of **1** in the presence of Ag⁺ ion (Fig. S15, ESI†).

The aggregation behavior was further supported by the optical image study of compound **1** at a conc. of 1×10^{-3} in DMF, DMF/H$_2$O (v/v, 1/1), and in the presence of 1 and 2 equiv. of Ag⁺ ion in DMF/H$_2$O (v/v, 1/1) solvent (Fig. S14, ESI†). It was observed that while in DMF, compound **1** was spread over on the cover slip, aggregation started to occur in DMF/H$_2$O, enlightening the role of water in the process. In comparison, fibril networks were observed in the presence of 1 and 2 equiv. of Ag⁺ ion (Fig. S16a and b, ESI†) and endowed the coordination role of Ag⁺ ions to allow aggregation in a different mode.

To check the coordination role of Ag⁺ ions in forming the gel, the interaction of the Ag⁺–gel of **1** with the halide ions (F⁻, Cl⁻, Br⁻, and I⁻ as potassium salt) was investigated. After 30 min of addition of the salts, partial or almost complete degradation of the gel was observed (Fig. 8). Degradation is minimum for F⁻ and the gel was almost transformed into a sol material in the presence of I⁻. This observation suggested that
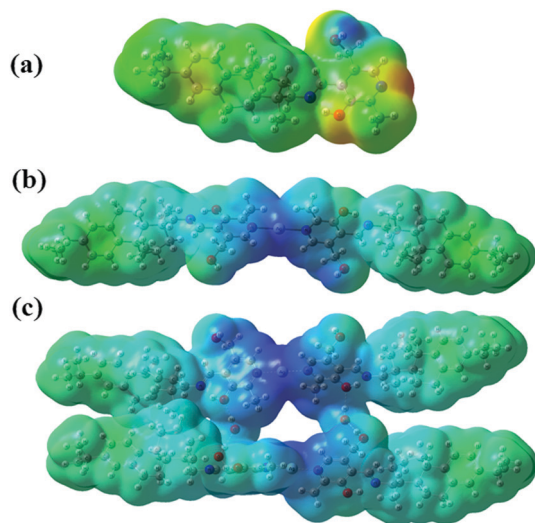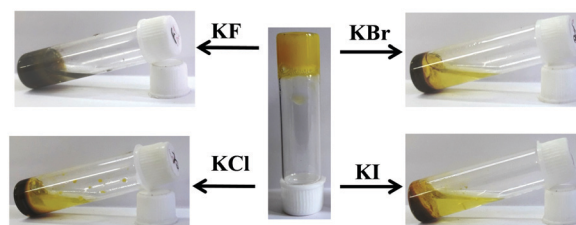

Fig. 6 MESP plots of (a) **1**, (b) dimer of **1** with Ag⁺, and (c) tetramer containing **1** and Ag⁺.

Fig. 8 Interaction of Ag⁺ gel of compound **1** with halide ions (F⁻, Cl⁻, Br⁻, and I⁻ as potassium salt).

the gel is formed due to Ag$^+$–ligand interaction. The scavenging of Ag$^+$ ions by halide ions from the gel matrix ruptures the gel.

In order to obtain information about the molecular chirality and chirality of supramolecular architecture during aggregation, the CD spectra of **1** in DMSO : H$_2$O (1 : 1, v/v) itself and in the presence of Ag$^+$ at different concentrations were compared with Ag$^+$–gel. While **1** showed weak positive and negative Cotton effects at about 294 nm and 350 nm, respectively, in aqueous DMSO suggesting weak helical conformation, there was no distinct CD signal initially in the presence of the Ag$^+$ ion at which there was no gel formation. But in the gel state, strong negative Cotton effect at approximately 317 nm and a moderate negative Cotton effect at 420 nm were observed (Fig. S17, ESI†). Such a strong Cotton effect was ascribed to the chirality transfer from the dehydroabietylamine pendant to the pyridoxal moiety upon gel formation, thus expressing aggregation-induced circular dichroism (AICD) property.[38]

Rheological study

The mechanical property of the Ag$^+$–gel was studied by oscillatory rheological experiment (amplitude sweep and frequency sweep). For this, gels were prepared by adding 0.5 mL of aqueous solution of AgNO$_3$ to 5 mg of compound **1** dissolved separately in 0.5 mL DMSO, DMF, and dioxane. All experiments were carried out at 25 °C. The study of the storage modulus (G') and loss modulus (G'') versus %strain (amplitude sweep) at a constant frequency of 1 Hz were first carried out to establish the linear viscoelastic region (Fig. 9(a)–(c)). The shear strain up to 2%, 2.5%, and 3% of 100 Hz is in the linear viscoelastic region for gels of compound **1** in the presence Ag$^+$ ion prepared in DMSO/H$_2$O (1 : 1, v/v), DMF/H$_2$O (1 : 1, v/v), and dioxane/H$_2$O solvents, respectively. Then, both G' and G'' started to decrease and respective crossover between G' and G'' was observed at 31%, 32%, and 33% strain, which indicated the loss of the gel property (Fig. 9(a)–(c)). The higher value of G' over G'' in the linear viscoelastic region demonstrated that the rheological property of the supramolecular gel is dominated by the elastic property over the viscous property. Frequency sweep

Table 1 Rheological properties of the gels of compound **1** formed in different solvent systems

Solvent system (1 : 1, v/v)	Critical strain (%)	Crossover (% strain)	G'_{av}(Pa)	G''_{av} (Pa)	Tan δ (G''_{av}/G'_{av})
DMSO–H$_2$O	2.0	31	15990	1797	0.11
DMF–H$_2$O	2.5	32	1782	342	0.19
Dioxane–H$_2$O	3.0	33	15990	1792	0.11

experiment was carried out at a constant strain of 0.5%, which is well below the deformation limit in the linear viscoelastic region. Frequency sweep experiment showed the independent nature of G' with respect to frequency (Fig. 9(d)–(f)). Table 1 reports the different attributes of the gels. Gels obtained from different solvents show comparable gel stiffness and strain-bearing capacity.

Gel stiffness is also associated with the nature of the metal salt used. In this context, the gel in the presence of AgOAc, as shown in Fig. S18 (ESI†), showed the different rheological property from that of the AgNO$_3$-induced gel. The G' and G'' started to decrease within a short span of strain and the crossover between G' and G'' was observed at 0.45% strain (Fig. S18, ESI†). This corroborated the less elastic character of the gel (i.e., weak gel; Table S2, ESI†) compared to the gel using AgNO$_3$.

Solution phase interaction

Solution phase interaction of **1** with aforementioned metal ions was also investigated by UV-vis, fluorescence, and ^{1}H NMR spectroscopic methods. However, the outcome was completely different from the gel phase study. UV-vis spectroscopic study of **1** in DMSO/H$_2$O (1 : 1, v/v) showed two distinct absorptions at 336 nm and 416 nm. The intensities of these two peaks were decreased in the presence of all metal ions except Hg^{2+} almost in equal magnitudes (Fig. 10a and Fig. S19, ESI†). Only Hg^{2+} brought about a significant change in UV-vis spectra, indicating the measurable interaction in solution, although there was no gel formation in its presence. In contrast, Ag$^+$ ion, in spite of its weak interaction in solution, gave gel formation presumably due to the feasibility of metal coordination geometry to form the 3D-network in solution. Fig. 11(a) represents the UV-vis titration spectra of **1** in DMSO/H$_2$O (1 : 1, v/v) in the presence of Hg^{2+}. In this study, upon the successive addition of Hg^{2+}, the intensity of absorptions at 336 nm and 416 nm gradually decreased and continued up to the addition of 3 equiv. of Hg^{2+} ion.

Solution phase interaction of **1** with metal ions was further investigated by fluorescence. Upon excitation at 322 nm, compound **1** in DMSO/H$_2$O (1 : 1, v/v) showed two emission maxima at 382 nm and 520 nm. Similar to the absorption spectra, compound **1** in DMSO/H$_2$O (1 : 1, v/v) did not show any significant change in the emission spectrum in the presence of Ag$^+$. However, a significant change in the emission was observed in the presence of Hg^{2+} (Fig. 10(b)). Upon the successive addition of 3 equiv. amounts of Hg^{2+}, both the emission bands gradually increased (Fig. 11(b)). There was no
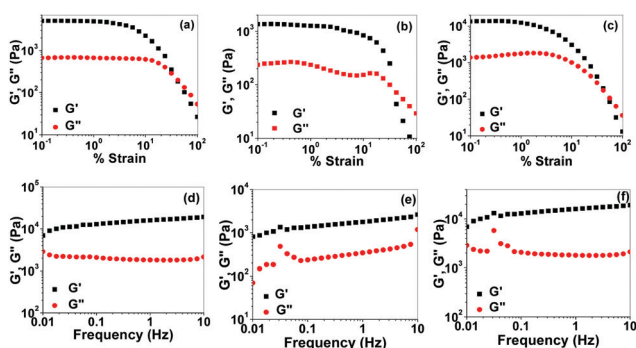

Fig. 9 Rheological behavior of supramolecular gel of **1**: storage modulus G' and loss modulus G'' of the gel on strain sweep prepared in (a) DMSO/H$_2$O (1 : 1, v/v), (b) DMF/H$_2$O (1 : 1, v/v), (c) dioxane/H$_2$O (1 : 1, v/v) solvent system, and storage modulus G' versus frequency sweep (strain: 0.5%) of the gel in (d) DMSO/H$_2$O (1 : 1, v/v), (e) DMF/H$_2$O (1 : 1, v/v), and (f) dioxane/H$_2$O (1 : 1, v/v) solvent system.
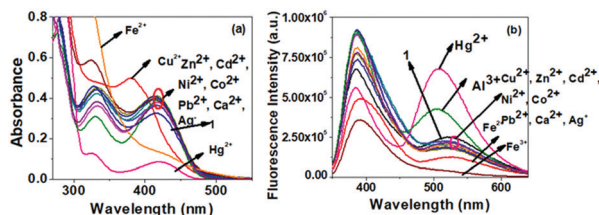
Fig. 10 Change in (a) absorption and (b) emission spectra of compound **1** ($c = 2.5 \times 10^{-4}$ M) in the presence of 3 equiv. of different metal ions ($c = 1 \times 10^{-3}$ M).
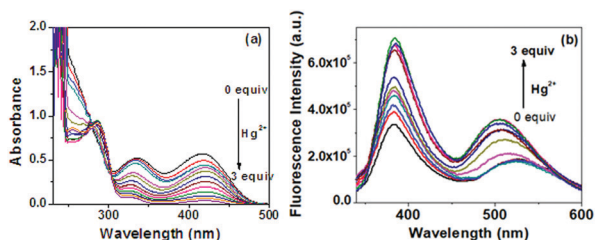

Fig. 11 (a) Absorption and (b) emission titration spectra of compound **1** in DMSO/H$_2$O (1:1, v/v) ($c = 2.5 \times 10^{-4}$ M) in the presence of Hg^{2+} ion ($c = 1 \times 10^{-3}$ M) (Hg^{2+} is taken as HgClO$_4$).

considerable change in the emission in the presence of the other metal ions (Fig. S20, ESI†). It is to be pointed out that compound **1** in low concentration (1.0×10^{-5} M) showed very small absorbance, which underwent a further decrease upon the successive addition of Hg^{2+}, leading to negative absorbance due to the dilution effect (Fig. S21a, ESI†). Although the spectral change was identical to that in Fig. 11(a), it was not considered in our study. Similar to that in UV-vis, in low concentration, compound **1** ($c = 1.0 \times 10^{-5}$ M) in fluorescence also exhibited weak emission at ∼400 nm, which was gradually intensified upon titration with Hg^{2+} and suggested its sensitivity toward Hg^{2+} (Fig. S21b, ESI†). The emission at ∼520 nm was too weak to detect. While the concentration of **1** is increased, it emerges with moderate intensity due to aggregation (Fig. S21c, ESI†).

To support the interaction of compound **1** with Hg^{2+}, the ^{1}H NMR spectrum of compound **1** in the presence of 1 equiv. and 3 equiv. of HgClO$_4$ was recorded in d$_6$-DMSO (Fig. S22, ESI†). In the presence of 1 equiv. of Hg^{2+}, both Ar–OH$_a$ and –CH$_2$OH$_b$ underwent downfield chemical shift by 0.74 and 0.22 ppm, respectively. Further, with the addition of Hg^{2+} up to 3 equiv., the downfield chemical shift of the said protons was increased by 0.29 and 0.06 ppm, respectively. The pyridine ring proton H$_c$ and H$_d$ proton from –CH$_2$OH also underwent downfield chemical shift (Fig. S22, ESI†). With this information in hand, it was assumed that the imino-phenol part of **1** is engaged in interaction with Hg^{2+} (Fig. S22, ESI†).

Binding constant and detection limit[39,40]

The binding stoichiometry of **1** with Hg^{2+} was determined to be 1:1 (H/G) in DMSO/H$_2$O (1:1, v/v), as indicated by the Benesi–Hildebrand plots (Fig. S23, ESI†). From UV-Vis titration spectra,

the value of $A_0/A - A_0$ *versus* 1/[G] plot at 420 nm showed good linear relationship with $R_2 = 0.997$ and association constant was calculated to be 2.72×10^3 M^{-1}. The detection limit for Hg^{2+} was calculated as 2.09×10^{-6} M (Fig. S24, ESI†).

Conclusion

In summary, a simple pyridoxal-based Schiff base progelator **1** has been designed, synthesized, and characterized. Compound **1** does not form gel in any organic solvent tested and formed precipitates in a series of organic solvents such as DMSO, DMF, dioxane, and acetonitrile. But it undergoes sol-to-gel transition in DMSO/H$_2$O, DMF/H$_2$O, dioxane/H$_2$O, and CH$_3$CN/H$_2$O selectively in the presence of Ag$^+$ ion and validates the selective naked eye detection of Ag$^+$ ion over a series of other metal ions. The Ag$^+$–gel has a fibrous morphology and shows good viscoelastic behavior. A theoretical study was done to explain the mode of aggregation. The absence of phenolic –OH and alcoholic –OH in model compound **2**, which is reluctant undergo gel formation under the conditions, proves the role of pyridoxal in **1** for gelation. Compound **1** does not show any specific interaction in solution with Ag$^+$ but reveals the selective recognition of Hg^{2+} ion by exhibiting considerable changes in the UV-Vis and fluorescence. The detection limit for Hg^{2+} was determined to be as low as 2.09×10^{-6} M. Thus, the present study on pyridoxal-based Schiff base in the detection of metal ions through gel formation is a new addition (Table S3, ESI†). In this context, no report except one from our laboratory is known in the literature. Even the use of dehydroabietylamine as a hydrophobic component in the fabrication of gelator is unknown except one example to date.[41]

Experimental

Material

Pyridoxal hydrochloride (99%), (+)-dehydroabietylamine (60%), and pyridine-4-carboxaldehyde were purchased from Sigma Aldrich and used as received. Nitrate salts of Ag^{2+}, Cu^{2+}, Pb^{2+}, Co^{2+}, Ni^{2+}, Cd^{2+}, Zn^{2+}, Hg^{2+}, and Fe^{3+}, and perchlorate salts of Ca^{2+}, Al^{3+}, Fe^{2+}, and Hg^{2+} were purchased from Sigma-Aldrich. CDCl$_3$ (99.8% D) and DMSO-d$_6$ (99.8% D) were purchased from Cambridge Isotope Laboratories, Inc., USA for NMR study. The solvents used in the experiments were purified and dried before use by standard procedures.

Instrumentation

^{1}H and ^{13}C NMR spectroscopic studies were conducted on a BrukerAvance IIII 400 spectrometer operating at 400 MHz. Mass spectrometry (ESI-MS) was conducted on a high resolution Agilent 6535 Q-TOF LC/MS mass spectrometer. The FT-IR spectroscopic study was conducted on KBr pellets using a PerkinElmer Spectrum L120-00A FT-IR Spectrometer. The UV-VIS spectra were recorded using a Shimadzu UV-2450 and fluorescence spectroscopic study was conducted using HORIBA FluoroMax-4C.

Synthesis

Compound 1. Triethylamine (Et_3N, 0.375 mL, 2.70 mmol) was added dropwise to a stirred solution of pyridoxal hydrochloride (0.5 g, 2.46 mmol) in CH_3OH (20 mL). After stirring for 10 min, dehydroabietylamine (0.70 g, 2.46 mmol) in 2 mL CH_3OH was added and the reaction mixture was boiled to reflux for 3.5 h. After the completion of the reaction, CH_3OH was removed by rotary evaporator and diethylether (50 mL) was added to the residue. The precipitation that appeared was filtered off and ether was removed under reduced pressure. The resulting residue was purified by column chromatography using ethyl acetate/pet ether eluent (7:3 v/v) to give a yellow powder of compound **1** (0.9 g, yield: 75%). m.p. 86 °C. ^1H NMR (400 MHz, $CDCl_3$): δ 14.33 (s, 1H), 8.75 (s, 1H), 7.33 (s, 1H), 7.09 (d, 1H, J = 8 Hz), 6.91 (d, 1H, J = 8 Hz), 6.78 (s, 1H), 4.69 (s, 2H), 3.47 (s, 2H), 2.82–2.71 (m, 3H), 2.42 (s, 3H), 2.22 (d, 1H, J = 12 Hz), 1.87–1.68 (m, 6H), 1.45–1.36 (m, 5H), 1,29–1.26 (m, 6H), 1.24 (s, 3H); ^{13}C NMR (100 MHz, $CDCl_3$): δ 162.80, 155.50, 151.13, 146.96, 145.60, 137.37, 134.49, 130.94, 126.82, 124.37, 123.96, 119.63, 71.84, 60.68, 46.22, 38.24, 37.98, 37.69, 36.68, 33.39, 29.68, 25.51, 23.92, 19.19, 18.93, 18.87 and 18.72; FT-IR (cm^{-1}): 3370, 2927, 2867, 2111, 1737, 1630, 1498, 1454, 1400, 1291, 1256, 1212, 1169, 1083, 1029, 886, 821, 784, 718; HR-MS: cal. for $[M+H^+]$ $C_{28}H_{38}N_2O_2H$: 435.3012, found 435.3009.

Compound 2. Pyridine-4-carboxaldehyde (0.2 g, 1.86 mmol) and dehydroabietylamine (0.568 g, 2.05 mmol) were dissolved in 20 mL CH_3OH and then the reaction mixture was heated to reflux for 4 h. After the completion of the reaction, CH_3OH was removed by a rotary evaporator and the resulting residue was purified by column chromatography using ethyl acetate/pet ether (6:4, v/v) as the eluent to yield a gummy colorless substance. ^1H NMR (400 MHz, $CDCl_3$): δ 8.68–8.64 (m, 2H), 8.22 (s, 1H), 7.59–7.56 (m, 2H), 7.18 (d, 1H, J = 8 Hz), 6.98 (d, 1H, J = 8 Hz), 6.86 (s, 1H), 3.56–3.40 (m, 3H), 2.87–2.77 (m, 2H), 2.26 (d, 1H, J = 12 Hz), 1.88–1.67 (m, 6H), 1.53–1.36 (m, 5H), 1.24–1.19 (m, 6H), 1.05 (s, 3H); ^{13}C NMR ($CDCl_3$, 100 MHz): δ 158.77, 150.36, 147.35, 145.46, 143.01, 134.81, 126.86, 124.43, 123.89, 121.96, 73.33, 45.86, 38.41, 38.26, 37.66, 36.70, 33.42, 30.49, 25.63, 23.98, 19.57, and 18.86 (one carbon in the aliphatic region is unresolved); FT-IR (cm^{-1}): 3391, 3092, 2890, 1696, 1664, 1612, 1587, 1568, 1504, 1458, 1433, 1399, 1342, 1366, 1269, 1231, 1159, 1128, 1053, 956, 881, 859, 839, and 778; anal. calcd for $C_{26}H_{34}N_2$: C, 83.37; H, 9.15; N, 7.48, found: C, 83.13; H, 9.35; N, 7.41.

General procedure for the gelation test

A measured amount of compound **1** was dissolved in pure organic solvents and all metal salts analytes were dissolved in deionized water. Then, 0.5 mL of 1 equiv. or 2 equiv. amounts of the metal solution was added to 0.5 mL solution of compound **1** to test the gel formation. The gel formation was tested *via* the inversion of vial method.

The anion responsive behavior of the metallogel was further tested *via* the degradation of the gel in the presence of equivalent amounts of halides.

Sample preparation for SEM and optical imaging

The SEM image of the gel sample was prepared by placing a thin layer of the gel sample on a cover slip and dried under high vacuum. Then, the dry gel sample was coated with a very thin layer of gold–palladium alloy and the image was recorded under SEM.

Optical imaging study of compound **1** in the absence and presence of Ag^+ was carried out using an optical microscope. For this purpose, compound **1** in DMF, DMF/H_2O (conc. = 1×10^{-3} M) and also compound **1** in DMF/H_2O (conc. = 1×10^{-3} M) in the presence of 1 and 2 equiv. of Ag^+ was drop-casted on the cover slip and dried.

General procedures for fluorescence and UV-vis titrations

A stock solution of compound **1** ($c = 2.5 \times 10^{-4}$ M) was prepared in DMSO:H_2O (1/1, v/v). Stock solutions of metal salts ($c = 1 \times 10^{-3}$ M) were also prepared in DMSO:H_2O (1/1, v/v). Then, 2 mL solution of compound **1** was taken in a cuvette and solutions of different metal salts were added individually in different amounts to record the change in absorbance and emission spectroscopy.

Binding constant determination[39]

The Benesi–Hildebrand plot was used to determine the stoichiometry of interaction using the expression: $A_0/(A - A_0) = [\varepsilon_M/(\varepsilon_M - \varepsilon_C)](K_a^{-1} C_g^{-1} + 1)$, where ε_M and ε_C denote the molar extinction coefficients for the probe and the complex, respectively, at a selected wavelength, A_0 denotes the absorbance of free compound at that specific wavelength, and C_g is the concentration of the metal ion analyte. The measured absorbance $A_0/(A - A_0)$ as a function of inverse of the analyte concentration fits a linear relationship, indicating a 1:1 stoichiometry of the probe–metal analyte complex. The ratio of slope to intercept was used to determine binding constant.

Calculation of detection limit[40]

The detection limit was calculated from the UV-vis titration data. The absorbance of compound **1** was measured five times, and the standard deviation of the blank measurement was calculated. To have the slope, the absorbance values of **1** *vs* concentrations of Hg^{2+} were plotted. The detection limit was calculated using the equation detection limit = $3\sigma/k$, where σ is the standard deviation of the blank measurement and k is the slope.

Computational details

All theoretical calculations have been performed using the density functional theory (DFT)-based Gaussian 09 program and calculated at the DFT/B3LYP 6-311++G(d,p) level in dimethyl sulfoxide (DMSO) solvent. The free ligand and its complex structure with silver ion were optimized using the same level of theory in DMSO solvent.

Conflicts of interest

There are no conflicts to declare.

Acknowledgements

References

1 A. Biswas, S. Mukhopadhyay, R. S. Singh, A. Kumar, N. K. Rana, B. Koch and D. S. Pandey, *ACS Omega*, 2018, **3**, 5417.

2 W. Ji, C. Yuan, S. Zilberzwige-Tal, R. Xing, P. Chakraborty, K. Tao, S. Gilead, X. Yan and E. Gazit, *ACS Nano*, 2019, **13**, 7300.

3 X. Yan, T. R. Cook, J. B. Pollock, P. Wei, Y. Zhang, Y. Yu, F. Huang and P. J. Stang, *J. Am. Chem. Soc.*, 2014, **136**, 4460.

4 M. O. M. Piepenbrock, N. Clarke and J. W. Steed, *Langmuir*, 2009, **25**, 8451.

5 Q. Tang, T. N. Plank, T. Zhu, H. Yu, Z. Ge, Q. Li, L. Li, J. T. Davis and H. Pei, *ACS Appl. Mater. Interfaces*, 2019, **11**, 19743.

6 A. De and R. Mondal, *ACS Omega*, 2018, **3**, 6022.

7 N. Alam and N. D. Sarma, *Soft Matter*, 2020, **16**, 10620.

8 P. Biswas and P. Dastidar, *Inorg. Chem.*, 2021, **60**, 3218.

9 K. Sarkar and P. Dastidar, *Chem. – Asian J.*, 2019, **14**, 194.

10 S. D. Kurbah and R. A. Lal, *New J. Chem.*, 2020, **44**, 5410.

11 N. Malviya, C. Sonkar, B. K. Kundu and S. Mukhopadhyay, *Langmuir*, 2018, **34**, 11575.

12 P. Das, S. Majumdar, A. Dey, S. Mandal, A. Mondal, S. Chakrabarty, P. P. Ray and B. Dey, *New J. Chem.*, 2021, **45**, 15920.

13 V. Kumar, R. K. Upadhyay, D. Bano, S. Chandra, D. Kumar, S. Jit and S. H. Hasan, *New J. Chem.*, 2021, **45**, 6273.

14 A. Panja, S. Ghosh and K. Ghosh, *New J. Chem.*, 2019, **43**, 10270.

15 S. Datta and S. Bhattacharya, *Chem. Soc. Rev.*, 2015, **44**, 5596.

16 (*a*) M. Martinez-Calvo, O. Kotova, M. E. Möbius, A. P. Bell, T. McCabe, J. J. Boland and T. Gunnlaugsson, *J. Am. Chem. Soc.*, 2015, **137**, 1983; (*b*) T. Feldner, M. Häring, S. Saha, J. Esquena, R. Banerjee and D. Diaz Diaz, *Chem. Mater.*, 2016, **28**, 3210; (*c*) M.-O. M. Piepenbrock, G. O. Lloyd, N. Clarke and J. W. Steed, *Chem. Rev.*, 2010, **110**, 1960; (*d*) W. Weng, A. M. Jamieson and S. J. Rowan, *Tetrahedron*, 2007, **63**, 7419.

17 R. Raza, N. Dey, A. Panja and K. Ghosh, *ChemistrySelect*, 2019, **4**, 11564.

18 W. Fang, Y. Zhang, J. Wu, C. Liu, H. Zhu and T. Tu, *Chem. – Asian J.*, 2018, **13**, 712.

19 A. Adhikary, K. S. Das, S. Saha, M. Roy and R. Mondal, *Dalton Trans.*, 2020, **49**, 13487.

20 H. Su, S. Zhu, M. Qu, R. Liu, G. Song and H. Zhu, *J. Phys. Chem. C*, 2019, **123**, 15685.

21 T. P. Huynh, P. Sonar and H. Haick, *Adv. Mater.*, 2017, **29**, 1604973.

22 A. Dutta, K. Ghosal, K. Sarkar, D. Pradhan and R. K. Das, *Chem. Eng. J.*, 2021, **419**, 129528.

23 W. Zhang, Z. Wang, L. Tao, K. Duan, H. Wang, J. Zhang, X. Pan and Z. Huo, *J. Solid State Electrochem.*, 2019, **23**, 1563.

24 C. Gu, J. Li, J. P. Liu, H. Wang, Y. Peng and C. S. Liu, *Appl. Catal., B*, 2019, **286**, 119888.

25 C. Mahendar, Y. Kumar, M. K. Dixit and M. Dubey, *Soft Matter*, 2020, **16**, 3436.

26 (*a*) A. Renzoni, F. Zino and E. Franchi, *Environ. Res.*, 1998, **77**, 68; (*b*) G. E. Mckeown-Eyssen, J. Ruedy and A. Neims, *Am. J. Epidemol.*, 1983, **118**, 470; (*c*) S. G. Roy, S. Mondal and K. Ghosh, *New J. Chem.*, 2020, **44**, 5921.

27 (*a*) I. Hoyle and R. D. Handy, *Aquat. Toxicol.*, 2005, **72**, 147; (*b*) M. Harada, *Crit. Rev. Toxicol.*, 1995, **25**, 1.

28 (*a*) K. Ginjupalli, T. Shaw, C. Tellapragada, R. Alla, L. Gupta and N. U. Perampalli, *Dent. Mater.*, 2018, **34**, 158; (*b*) Y. Niu, T. Guo, X. Yuan, Y. Zhao and L. Ren, *Soft Matter*, 2018, **14**, 1227.

29 *Silver catalysis in organic synthesis*, ed. C. J. Li and X. Bi, John Wiley & Sons, 2019.

30 Y. Zhu, K. Huang, J. Pan, X. Qiu, X. Luo, Q. Qin, J. Wei, X. Wen, L. Zhang and N. Jiao, *Nat. Commun.*, 2018, **9**, 1.

31 M. Zhao, D. Li, J. Huang, D. Wang, A. Mensah and Q. Wei, *J. Mater. Chem. C*, 2019, **7**, 13468.

32 Y. Okawa, T. Shimada and F. Shiba, *J. Electroanal. Chem.*, 2018, **828**, 144.

33 A. U. Rehman, Y. Wu, H. D. Tran, K. Vazquez-Prada, Y. Liu, H. Adelnia, N. D. Kurniawan, M. N. Anjum, S. S. Moonshi and H. T. Ta, *ACS Appl. Nano Mater.*, 2021, **4**, 10136.

34 (*a*) K. Ghosh, S. Panja and S. Bhattacharya, *ChemistrySelect*, 2017, **2**, 959; (*b*) S. Ghosh, A. Panja and K. Ghosh, *ChemistrySelect*, 2020, **5**, 5099; (*c*) G. K. Veits, K. K. Carter, S. J. Cox and A. J. McNeil, *J. Am. Chem. Soc.*, 2016, **138**, 12228.

35 F. Mandegani, H. Zali-Boeini, Z. Khayat, J. D. Braun and D. E. Herbert, *ChemistrySelect*, 2020, **5**, 886.

36 A. Panja and K. Ghosh, *New J. Chem.*, 2019, **43**, 5139.

37 M. J. Frisch, G. W. Trucks, H. B. Schlegel, G. E. Scuseria, M. A. Robb, J. R. Cheeseman, G. Scalmani, V. Barone, B. Mennucci, G. A. Petersson, H. Nakatsuj, M. Caricato, X. Li, H. P. Hratchian, A. F. Iamaylov, J. Bloino, G. Zheng, J. L. Sonnenberg, M. Hada, M. Ehara, K. Toyota, R. Fukuda, J. Hasegawa, M. Ishida, T. Nakajima, Y. Honda, O. Kitao, H. Nakai, T. Vreven, J. A. Montgomery Jr, J. E. Peralta, F. Ogliaro, M. Bearpark, J. J. Heyd, E. Brothers, K. N. Kudin, V. N. Staroverov, R. Kobayashi, J. Normand, K. Raghavachari, A. Rendell, J. C. Burant, S. S. Lyengar, J. Tomasi, M. Cossi, N. Rega, J. M. Millam, M. Klene, J. E. Knox, J. B. Cross, V. Bakken, C. Adamo, J. Jaramillo, R. Gomperts, R. E. Stratmann, O. Yazyev, A. J. Austin, R. Cammi, C. Pomelli, J. W. Ochterski, R. L. Martin, K. Morokuma, V. G. Zakrzewski, G. A. Voth, P. Salvador, J. J. Dannenberg, S. Dapprich, A. D. Daniels, O. Farkas, J. B. Foresman, J. V. Ortiz, J. Cioslowski and D. J. Fox, *Gaussian 09, Revision A.1*, Gaussian Inc., Wallingford CT, 2009.

38 C. Yu, M. Xue, K. Liu, G. Wang and Y. Fang, *Langmuir*, 2014, **30**, 1257–1265.

39 P. T. Chou, G. R. Wu, C. Y. Wei, C. C. Cheng, C. P. Chang and F. T. Hung, *J. Phys. Chem. B*, 2000, **104**, 7818–7829.

40 A. R. Sarkar, C. H. Heo, M. Y. Park, H. W. Lee and H. M. Kim, *Chem. Commun.*, 2014, **50**, 1309–1312.

41 A. Aslam, I. Ali Hashmi, V.-U. Ahmed and F. I. Ali, *Synth. Commun.*, 2013, **43**, 2824.